Since January 2020 Elsevier has created a COVID-19 resource centre with free information in English and Mandarin on the novel coronavirus COVID-19. The COVID-19 resource centre is hosted on Elsevier Connect, the company's public news and information website.

Science of the Total Environment 769 (2021) 145527

Contents lists available at ScienceDirect

Science of the Total Environment

journal homepage: www.elsevier.com/locate/scitotenv

Repurposing of COVID-19 single-use face masks for pavements base/subbase

Mohammad Saberian, Jie Li *, Shannon Kilmartin-Lynch, Mahdi Boroujeni

School of Engineering, RMIT University, Melbourne, Victoria, Australia

HIGHLIGHTS

- A new and low carbon strategy is proposed to reduce pandemic-generated waste.
- The inclusion of shredded face mask can improve ductility, flexibility and strength.
- The disposed face masks can be used for pavement base/subbase applications.

GRAPHICAL ABSTRACT

ARTICLE INFO

Article history:
Received 8 November 2020
Received in revised form 25 January 2021
Accepted 26 January 2021
Available online 1 February 2021

Editor: Damia Barcelo

Keywords:
COVID-19
Waste management
Face masks
Polypropylene plastic
Recycled concrete aggregate
Pavement geotechnics

ABSTRACT

The coronavirus (COVID-19) pandemic has not only created a global health crisis, but it is also now threatening the environment. A multidisciplinary collaborative approach is required to fight against the pandemic and reduce the environmental risks associated with the disposal of used personal protective equipment (PPE). This paper explores an innovative way to reduce pandemic-generated waste by recycling the used face masks with other waste materials in civil constructions. In this research, for the first time, a series of experiments, including modified compaction, unconfined compression strength and resilient modulus tests, were conducted on the blends of different percentages of the shredded face mask (SFM) added to the recycled concrete aggregate (RCA) for road base and subbase applications. The experimental results show that RCA mixed with three different percentages (i.e., 1%, 2% and 3%) of SFM satisfied the stiffness and strength requirements for pavements base/subbase. The introduction of the shredded face mask not only increased the strength and stiffness but also improved the ductility and flexibility of RCA/SFM blends. The inclusion of 1% SFM to RCA resulted in the highest values of unconfined compressive strength (216 kPa) and the highest resilient modulus (314.35 MP). However, beyond 2%, increasing the amount of SFM led to a decrease in strength and stiffness.

1. Introduction

During the coronavirus (COVID-19) pandemic, the use of personal protective equipment (PPE) such as face masks and plastic gloves has risen sharply (Daryabeigi Zand and Vaezi Heir, 2020; Klemeš et al., 2020; Ludwig-Begall et al., 2020; Prata et al., 2020; Silva et al., 2020; Zambrano-Monserrate et al., 2020; Boroujeni et al., 2021). Many countries have implemented mandatory requirements for wearing face masks in public. The use of face masks by general populations can reduce the spread of COVID-19, but it also causes severe problems for the environment. It is estimated that the daily face mask use in Africa is more than seven hundred million, while this number is more than 2.2 billion in Asia every day (Nzediegwu and Chang, 2020; Rowan and Laffey, 2020; Sangkham, 2020). To the best knowledge of the authors, there is no up to date statistics of the daily number of face mask use

* Corresponding author.
E-mail addresses: mohammad.boroujeni@rmit.edu.au (M. Saberian), jie.li@rmit.edu.au (J. Li), shannon.kilmartin-lynch@rmit.edu.au (S. Kilmartin-Lynch), mahdisaberian@rocketmail.com (M. Boroujeni).

https://doi.org/10.1016/j.scitotenv.2021.145527
0048-9697/

around the world; however, it was estimated in June 2020 that monthly, 129 billion face masks were discharged into the environment (Prata et al., 2020). These numbers come back to the dates before the mandatory face mask policies enforced in several countries around the world. Thus, it is anticipated that currently, the global use of face masks is more than 129 billion every month due to the COVID-19 pandemic. Using the model of the daily global face mask proposed by Nzediegwu and Chang (2020), the authors estimate that 6.88 billion (approximately 206,470 t) face masks are generated around the world each day, which are ultimately sent to landfills or incinerated.

Unfortunately, used face masks can be spotted almost everywhere from city streets to car parks to local parks because of an uptick in littering. Even if the masks are thrown in trash bins or sit in landfill sites, due to the lightweight nature of the masks, wind and rainwater can move the masks freely into city streets or rivers and oceans, where the plastic-based masks can be fragmented into microplastics. Thus, throwing away the masks or improper waste management of the used personal protective equipment can end up causing problems for wildlife or killing animals and marine life (Fadare and Okoffo, 2020; Hirsh, 2020; Prata et al., 2020). Furthermore, the single-use masks are made of non-biodegradable plastics, which means that they take hundreds of years to break down in the environment (Dhawan et al., 2019). Therefore, multidisciplinary collaboration is urgently required to fight against the COVID-19 pandemic and reduce the environmental risks associated with the disposal of used PPE.

On the other hand, the consumption of quarry aggregates has increased significantly due to increasing activities in civil and infrastructure sectors (Saberian et al., 2021). Consequently, large amounts of natural resources are being used in civil engineering. Besides, the extraction of virgin materials results in large quantities of greenhouse gas emissions (Saberian et al., 2019a). Moreover, the construction sector, compared to the other waste generators, is responsible for the generation of significant amounts of waste materials (i.e. almost about half of the global generated wastes), which are mainly produced by demolishing buildings and other infrastructure projects (AzariJafari et al., 2016; Saberian and Li, 2019; Kazemi et al., 2020; Hajforoush et al., 2019). Fortunately, to alleviate the negative environmental impact caused by the wastes, the possibility of recycling and reusing construction and demolition waste in civil engineering projects has significantly surged (Li et al., 2018a; Lei et al., 2018). Construction and demolition waste comprises a wide variety of materials including recycled concrete aggregate, reclaimed asphalt pavement, crushed brick, crushed glass and crushed rock. Among these, concrete waste is produced from the construction and demolition activities of concrete structures (Saberian et al., 2019d). The concrete waste constitutes a significant proportion of the construction and demolition wastes at about 45%. Recycled concrete aggregate (RCA) is obtained from crushing the concrete chunks into aggregates. The 20 mm nominal size of RCA is generally used in pavement applications (Saberian et al., 2020b).

In order to reduce the negative environmental impacts caused by the pandemic, urgent multidisciplinary collaborations are required. The environmental geotechnics scientific community can utilize its long-term accumulated professional skills to make important contributions to fight against the COVID-19 pandemic. Using sterilized waste materials in geotechnical applications has been suggested to be an effective way to address the waste management issues caused by the pandemic (Tang et al., 2020).

2. Significance of research

The outbreak of the COVID-19 pandemic has created not only a global health and financial crisis but also an unprecedented impact on the environment. An enormous amount of PPE is produced and used every day worldwide, which is eventually sent to landfills or incinerated. To date, few studies have been conducted to tackle COVID-generated waste. This research proposes an innovative way to reduce pandemic-generated waste by recycling and reusing the shredded face mask (SFM) and mixing with recycled concrete aggregate (RCA) for pavement constructions. For the first time, a series of experiments, including modified compaction test, unconfined compression strength test and resilient modulus test, was performed to evaluate the feasibility of using SFM with RCA as road pavement materials. The outcomes of this study can provide practical guidance on the application of SFM and RCA.

3. Materials and methods

The used face masks were not allowed to use in laboratory testing due to the laboratory work safety rules and restrictions during COVID-19 pandemic. Therefore, clean surgical face masks were used in the experimental program and shredded to the sizes of 0.5 cm width and 2 cm length. Supplementary File 1 illustrates a view of the shredded face mask (SFM) adopted in the current study. It should be pointed out that the metal strips and earloops were removed from the masks. In terms of the physical properties of the masks, top and bottom layers of the face masks were made of non-woven fabric (spunbond) while the middle layer of the masks was meltdown polypropylene.

A commercial RCA (i.e., Class II 20 mm) was utilized in this study as the aggregate for pavements base/subbase applications. It was collected from a recycling plant in Victoria, Australia. The physical appearance of RCA used in experimental testing is shown in Supplementary File 1. The RCA was oven-dried for at least one day in an oven with a temperature of 105 °C (Saberian et al., 2020c).

Regarding the sample preparation, the shredded face masks were mixed with dry RCA by 1%, 2%, and 3% (percentage by weight). This is in agreement with the inclusion of plastic fibers in pavement geotechnics, ranging from 0 to 5% (by weight% of soils) (Yaghoubi et al., 2017; Mishra and Gupta, 2018). Table 1 presents the four mixes of RCA and shredded face mask utilized in the current research.

The necessary precautions were taken to obtain a sample incorporating representative particle sizes and all conditions, as suggested by ASTM D75-03 (2014). The experimental testing for basic characterization purposes of RCA included particle size distribution test, organic content test, particle density test, specific gravity test, pH test, Los Angeles (LA) abrasion test, aggregate crushing value test, and flakiness index test. Moreover, the laboratory test program of basic characterization of the shredded face mask consisted of the tensile strength test, water absorption, melting point, and specific gravity. Moreover, the modified Proctor compaction, unconfined compression strength, and Repeated Load Triaxial (RLT) tests were undertaken on the blends of RCA and SFM at the room temperature of 20 ± 1 °C.

Particle size distribution tests were conducted on the blends, according to AS 1289.3.6.1 (2009). The utilized sieves had the aperture sizes ranging from 75 μm to 26 mm. For each mixture, a 2 kg sample was sieved before the compaction to be able to draw the particle size distribution curves, as per mentioned in the standard. ASTM D2487-17 (2017) was adopted to classify RCA based on the Unified Soil Classification System (USCS). RCA was tested for obtaining the values of pH, specific gravity, organic content, fine particle density, coarse particle density, and flakiness index according to the AS 1289.4.3.1 (1997), ASTM D854-10 (2010), ASTM D2974-14 (2014), AS 1141.5.1 (2000), AS 1141.6.1 (2000), and AS 1141.15 (2018) standards, respectively.

Table 1
The mixes considered for the experimental program.

Mix composition	Mix name
100% RCA (control sample)	100RCA
99% RCA + 1% SFM	99RCA1SFM
98% RCA + 2% SFM	98RCA2SFM
97% RCA + 3% SFM	97RCA3SFM

Degradation and crushing of aggregates such as RCA are significant for geotechnical and pavement applications (Saberian et al., 2020a). Therefore, Los Angeles abrasion test (AS 1141.23, 2009) and aggregate crushing value test (AS 1141.21, 1997) were also conducted on RCA.

The tensile strength test was conducted on the shredded surgical face masks using a universal testing machine at room temperature following ASTM D638-14 (2014) to measure the mechanical properties of the shredded face masks, including maximum tensile strength, tensile strength at break, rupture force, and elongation at break. The loading rate and load cell of the machine were set at 50 mm/min and 1 kN, respectively. The test was undertaken on five replicate pieces, and the average value of the five samples was reported. Besides, water absorption, 24 h at 23 °C, and melting point tests were conducted according to ASTM D570-98 (2018) and ASTM D7138-16 (2016), respectively. Moreover, ASTM D792-20 (2020) was followed to determine the specific gravity of the SFM.

Modified Proctor compaction test was conducted on the four blends following AS 1289.5.2.1 (2017) to measure the maximum dry density (MDD) and optimum moisture content (OMC) of each blend. The dry RCA was mixed with SFM and water at different water contents for 5 min by a commercial Hobart mixer. The blends were then sealed in plastic bags for a minimum of 2 h to allow the absorption of free water, according to AS 1289.5.2.1 (2017). This pre-curing treatment was also followed for the sample preparations for the UCS and RLT tests. To avoid segregation, the methods recommended by Yaghoubi et al. (2017) was followed, so that for each layer, the mixed materials were poured inside the mold by keeping the scoop very close to the top layer of the sample inside the mold. Besides, to visually evaluate the uniformity of the blends, random scoops of the mixtures were collected from the batches and spread on a table. No major differences in the shredded face mask contents were observed in each random extraction. The uniformity of the mixture of the RCA and shredded face mask can also be observed in Supplementary File 2, which shows a batch of a blend before the compaction and a sample after the testing (breakage was done by hand after the completion of the test). Therefore, it can be assured that the shredded mask pieces were mixed properly with RCA and evenly distributed in the compacted samples. It is worthy to note that three replicate identical samples were adopted and tested for each mixture for the mechanical testing of compaction, unconfined compression strength, and RLT tests.

With respect to the unconfined compression strength, the samples were prepared at their OMC, obtained from the compaction test results, and compacted in 5 layers and 25 number of blows per layer in the relevant compression strength mold with the height and diameter of 11.55 cm and 10.5 cm, respectively, according to the AS 5101.4 (2008). After extrusion from the mold, the samples were tested by a universal Shimadzu testing machine with a loading rate of 1.0 ± 0.1 mm/min. The average value of three replicate samples was reported.

Resilient modulus (M_r) is one of the most critical parameters required for the structural design of different pavement layers (Saberian and Li, 2018). Therefore, the determination of the resilient characteristics of granular aggregates as base and subbase materials is critical. The resilient behaviour of the blends was evaluated using RLT test, which simulates the condition of pavement layers under repeated traffic loading, in accordance with the AASHTO T307-99 standard (AASHTO, 2007). The RLT samples were compacted in a mold with a height of 200 mm and a diameter of 100 mm. Then, a triaxial cell with the universal testing machine was utilized to measure the M_r under a variety of stress and loading conditions comprising of 1 s haversine-shaped loading pulse with respective 0.1 s and 0.9 s loading and unloading periods. Except for the conditioning stage, which had 1000 loading cycles, each of the other 15 test stages of the RLT tests involved 100 loading cycles. The average of the last five cycles of all the stages for triplicate samples of each blend was reported as the M_r value.

4. Results and discussion

Supplementary File 3 illustrates the particle size distribution curves of the mixtures before the compaction. The blends are classified as GW-GC well-graded gravel with clay and sand, according to the Unified Soil Classification System (USCS) (ASTM D2487-17, 2017). Well-graded gravels can sustain large deviatoric stresses due to having higher contact areas which result in higher M_r values. Also, as can be seen from Supplementary File 3, the blends fitted within the upper- and lower-bound limits of the standard specifications for Type 1 gradation C material for base and subbase specified by ASTM D1241-15 (2015).

According to Supplementary File 4, which provides RCA's geotechnical properties, the aggregate has an organic content of 3.11%, which is mainly because of wooden particles from the construction and demolition activities. Moreover, the pH value of RCA, which is higher than 7, replicates that the aggregate is alkaline by nature. For pavement base/subbase materials, the maximum allowable value of both Los Angeles abrasion and flakiness index is 35% as specified by the guideline of the State road authority in Victoria, Australia (VicRoads, 2017). Also, the maximum limit for the aggregate crushing value is specified by 35% as per suggested by IS-2386 Part IV (1963). As can be seen from the Supplementary File 4, all the three mentioned properties of RCA are well below the limits recommended by the state road authorities as pavement base/subbase material.

Table 2 summarizes the physical properties of the SFM. The SFM was very light with a much lower specific gravity compared to the RCA. The tensile strength test on the SFM showed that the middle layer of the SFM, which is the polypropylene layer, contributed to most of the tensile strength.

The aspect ratio is defined as the length to the diameter of a fiber. The plastic fibers are classified to two categories of (a) short fibers or discontinuous fibers with an aspect ratio of between 20 and 60, and (b) long fibers or continuous fibers with an aspect ratio of more than 200. Long fibers are usually more difficult to disperse uniformly in a sample and more expensive to produce while short fibers can typically provide better strength and stiffness properties (Mishra and Gupta, 2018). According to Naaman (2003), the aspect ratio of a fiber with a non-circular cross-section can be calculated as:

$$\text{Aspect ratio} = \frac{l}{d_{FIER}} = \frac{l}{4\frac{A}{\Psi}} \quad (1)$$

where l is the length, d_{FIER} is the equivalent diameter, A is the cross-sectional area, and Ψ is the perimeter of the fiber cross-section of the fiber. The length, width, and thickness of the SFM used in this study were 20 mm, 5 mm, and 0.46 mm, respectively. Therefore, the aspect ratio of SFM is about 24. Thus, the SFM adopted in this study can be classified as short or discontinuous fiber.

4.1. Modified compaction test results

Fig. 1 illustrates the modified Proctor compaction test results in terms of the changes in the optimum moisture content (OMC %) and maximum dry density (MDD Mg/m^3) due to the inclusion of different

Table 2
Physical properties of SFM.

Physical properties	SFM
Specific gravity	0.91
Melting point (°C)	160
Water absorption 24 h (%)	8.9
Tensile strength (MPa)	4.25
Tensile strength at break (MPa)	3.97
Elongation at break (%)	118.9
Rupture force (N)	19.46
Aspect ratio	24

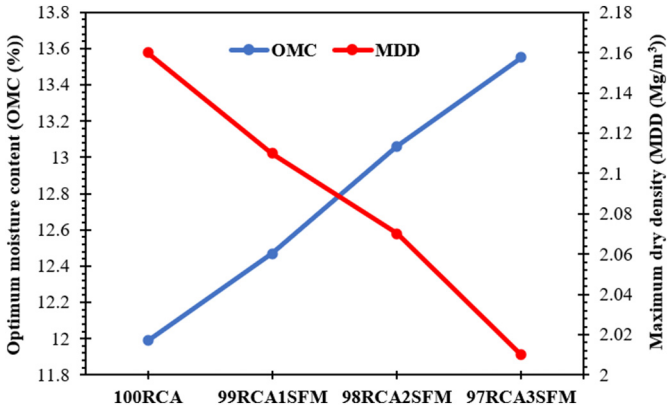

Fig. 1. Test results of modified Proctor compaction.

percentages of SFM. As the amount of SFM was increased from 0 to 3%, the OMC increased from 11.99 to 13.56%, while the MDD reduced from 2.16 to 2.01 Mg/m^3. The reduction in the MDD can be attributed to the lower specific gravity of the SFM compared to that of the RCA. A similar trend was also observed by Yaghoubi et al. (2017) and Perera et al. (2019) on the addition of polyethylene terephthalate, low-density polyethylene, and high-density polyethylene to the aggregates.

4.2. Unconfined compression test results

The unconfined compression test is one of the most popular tests in pavement geotechnics to evaluate the strength of pavement materials (MolaAbasi et al., 2019). Fig. 2 provides unconfined compressive strength (UCS) results of the blended samples with the error bars. Compared to the control sample (i.e., 0% SFM), the UCS value of 99RCA1SFM (1% SFM) increased by 17% (from 185 to 216 kPa). This is because SHM fibers played a reinforcing role in binding the RCA particles. The reinforcing mechanism of short and discrete SFM fibers is similar to that of polypropylene-reinforced or plastic fiber-reinforced soils. The introduction of randomly distributed SFM fibers would enhance the stretching resistance between aggregates.

Consequently, the strength of the RCA mixed with the SFM fibers would increase. A similar trend was observed in previous studies on the strength properties of polypropylene-reinforced clay soils (Zaimoglu, 2010; Tomar et al., 2020). The potential effects of short plastic fibers with low aspect ratio on the compressive strength of clay soil were also evaluated by Mishra and Gupta (2018). Fig. 2 shows that an addition of 1% SFM provided the highest UCS value (216 kPa). As the SFM was increased to 2% and 3%, the UCS of the blends reduced to 204 kPa and 178 kPa, respectively, indicating that there is a threshold value of SFM content beyond which the UCS reduced. Therefore, although an introduction of the SFM improved the integrity and strength of the RCA, increasing the SFM content would lead to decreasing UCS because the excessive fiber inclusion would result in the loss of stiffness of the blended sample due to high amount of voids. This is consistent with previous studies on the polypropylene-reinforced clay soil (Chen et al., 2015). Also, it can be stated that with the SFM content beyond 2%, the quantity of RCA matrix available for holding the fiber is insufficient to develop an effective bond between fibers and the RCA resulting in balling of fibers and poor mixing. A similar observation was also made by Pradhan et al. (2012) on the effect of random inclusion of polypropylene fibers on strength characteristics of cohesive clay soil. They reported that the inclusion of more than 1% of the fibers to the soil led to some difficulties in the soil compaction since the fibers stuck together and formed lumps, which caused pockets of low density.

Furthermore, Fig. 3 shows the bridge effect of the SFM in an underloaded situation of RCA sample along with the expansion and the deformation of the RCA. As can be seen, the SFM fibers played a reinforcing role in binding the RCA particles, and therefore, the bridging effect of the fibers in the RCA could obstruct the further development of tension cracks. Similar results on reinforced soils with polypropylene fibers were reported by Tomar et al. (2020) and Bojnourdi et al. (2020).

Fig. 2 shows the changes in the deformability of the samples as well. The flexibility of pavement layers is very important for flexible pavements (Saberian et al., 2019c). The flexibility can be evaluated by Eq. (2), which formulates the deformability index (I_D) that is the ratio of the failure strain of a given sample incorporating an additive ($\varepsilon_{f\ SFM}$) to the failure strain of the control sample ($\varepsilon_{f\ co}$) (Jahandari et al., 2019). According to the I_D results, the inclusion of the SFM into the RCA led to increasing the deformability index. This can be related to the higher tensile strength of the SFM with more flexibility compared to the RCA particles. In fact, by the introduction of the SFM fibers to the RCA, the strain at the failure tends to happen at higher strain levels due to the mobilization of the tensile strength of the SFM fibers. This finding is in agreement with previous results of Correia et al. (2015) and Venda Oliveira et al. (2018).

$$I_D = \varepsilon_{f\ SFM}/\varepsilon_{f\ co} \tag{2}$$

4.3. Resilient modulus (M_r) results

Fig. 4 provides the resilient modulus results of the samples. The M_r values are the average of the resilient modulus values from 15 stages of RLT test. Also, this figure compares M_r values of the RCA and the blends of the SFM-reinforced RCA with the recommended ranges of M_r for the pavement base (79–329 MPa) and subbase (42–228 MPa)

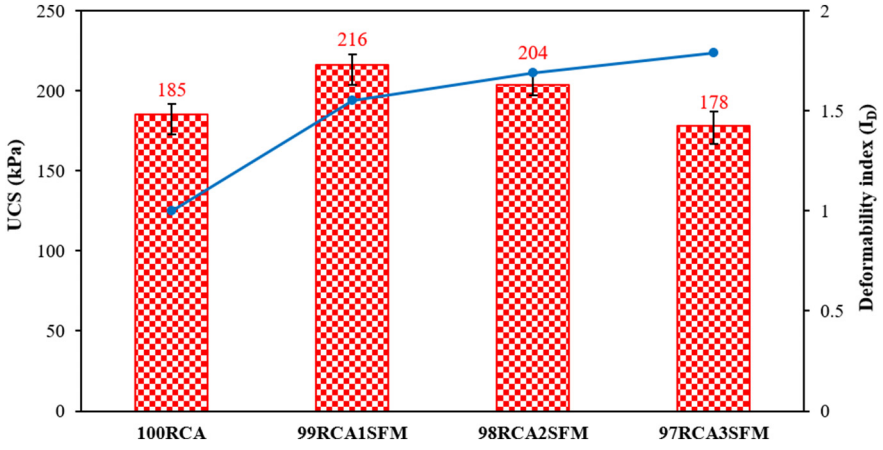

Fig. 2. UCA and I_D results of the blends.

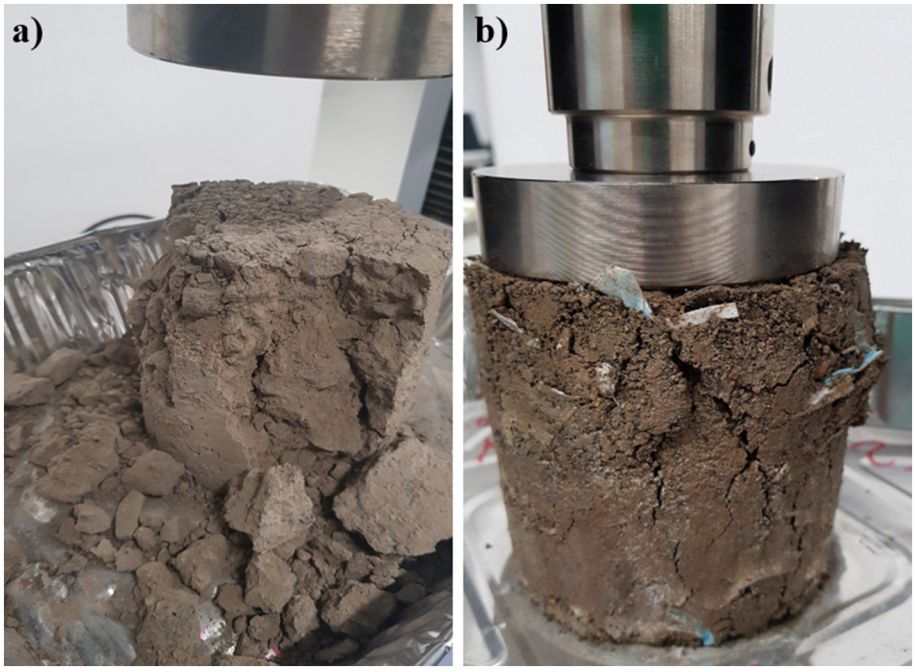

Fig. 3. The bridge effect of SFM fiber reinforcement in RCA that impeded the further development of tension cracks.

(AASHTO, 1993; Saberian et al., 2019b). It was found that the M_r value was highly dependent on the axial cyclic stress and confining stress. Similar to the UCS results, the inclusion of 1% SFM to RCA provided the highest M_r result at 314.35 MPa. In other words, the optimal SFM content was 1% by the dry weight of RCA. The increase in M_r values can be attributed to the increased stretching resistance between RCA particles by the inclusion of short SFM fibers. Further increasing of the SFM content led to a decrease in M_r, due to the high amount of voids and tangling of the excessive SFM fibers together in some parts of the samples that obstructed bonding between the fibers and RCA particles.

To evaluate the data obtained from the experimental testing results, two popular M_r prediction models were considered in this study. The models were the bulk stress model (AASHTO, 2007) and the three-parameter model (Puppala et al., 2011). The bulk stress model, as shown in Eq. (3), is one of the most suitable models for the prediction of M_r of granular materials like RCA (AASHTO, 2007). Previous studies found that confining pressure and deviator stress could have contradicting effects on resilient modulus of granular materials (Puppala et al., 2011; Li et al., 2018b; Saberian and Li, 2021). Therefore, Puppala et al. (2011) suggested a three-parameter model which separately considers the effects of deviator stress and confinement, as shown in Eq. (4).

$$M_r = k_1 \times \theta^{k}{}_2 \tag{3}$$

$$M_r = \sigma_{atm} \times k_3 \left(\frac{\sigma_3}{\sigma_{atm}}\right)^{k_4} \times \left(\frac{\sigma_d}{\sigma_{atm}}\right)^{k_5} \tag{4}$$

where $\theta = \sigma_1 + \sigma_2 + \sigma_3 = 3\sigma_3 + \sigma_d$; σ_{atm} is the atmospheric pressure; σ_d is the deviator stress; σ_3 is the confining pressure; k_1, k_2, k_3, k_4 and k_5 are regression constants. Table 3 presents the regression parameters of the three-parameter model and bulk stress model of the samples.

Fig. 5 shows comparisons between the measured M_r from the laboratory and the predicted M_r using the three-parameter model and bulk stress model. Based on the results, it can be concluded that the test data demonstrated an excellent fit for both models. In fact, the accuracy of the predictions with both models is noticeably high ($R^2 > 0.99$). This implies that the existing models can also be used to predict or evaluate the resilient behaviour of RCA reinforced with SFM fibers.

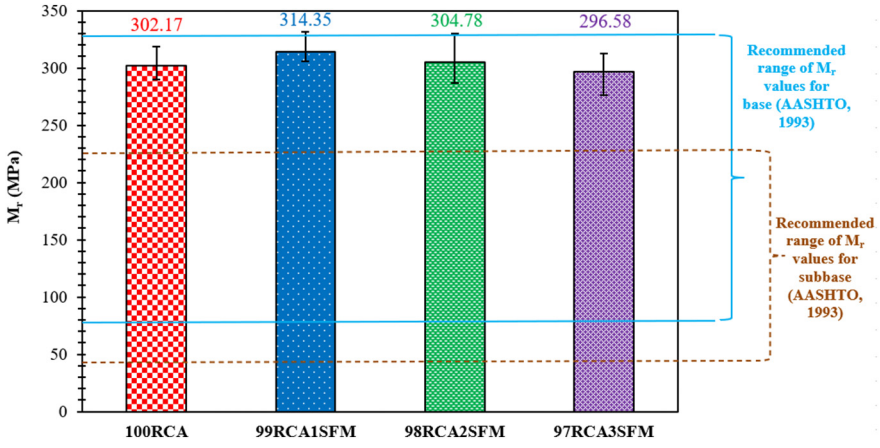

Fig. 4. Comparison of the M_r values of the samples.

Table 3
Regression parameters of the three-parameter model and bulk-stress model of the samples.

Sample	Bulk-stress model			Three-parameter model			
	K_1	K_2	R^2	K_1	K_2	K_3	R^2
100RCA	2.817	0.812	0.979	3.674	0.511	0.311	0.974
99RCA1SFM	3.683	0.774	0.968	3.796	0.478	0.306	0.961
98RCA2SFM	2.178	0.858	0.989	3.716	0.537	0.332	0.985
97RCA3SFM	1.651	0.899	0.985	3.599	0.532	0.386	0.985

4.4. Limitations of the study

The methodology proposed in the current study would be restricted to pavements and not building materials. Although the research has reached its aims, there was a potential limitation. Due to COVID-19 restrictions, we were not allowed to employ used face masks in the laboratory testing. Instead, clean face masks were used in the experimental program.

There are several methods available for disinfecting and sterilizing the face masks for reuse or before disposing. Ilyas et al. (2020) conducted a comprehensive review of the disinfection technologies to control/prevent the novel coronavirus spread and the proper management of COVID-waste. Doan (2020) recommended the microwaved method for disinfecting disposable medical masks. In this method, an antiseptic solution (i.e., 0.9% physiological saline) must be sprayed on the masks to maintain the moisture. Then, the moist masks have to be heated in a microwave oven, having a default capacity of 800 W, for about 1 min. It is worth to mention that the sprayed sides of the masks have to be faced up. This sanitizing method can effectively kill 99.9% of viruses (Doan, 2020). Xiang et al. (2020) reported that dry heat at both 60 °C and 70 °C for 1 h could ensure the decontamination of the surgical face mask while maintaining its filtering efficiency. Ultraviolet germicidal irradiation and hydrogen peroxide plasma can also be used for the inactivation of SARS-CoV-2 from the masks (Barcelo, 2020; Hamzavi et al., 2020; Ibáñez-Cervantes et al., 2020). To eliminate the risk of exposure to the COVID-19 virus during transportation and construction, it is suggested to keep face masks, after the disinfecting, in an open and restricted area, and exposed to sun and air for a week prior to pavement construction. Delivery trucks should be covered with tarps or a similar covering used to prevent dust. Trucks and road construction machinery need to be disinfected by using good hygiene practices and safe cleaning techniques. Since the main aim of this study is to evaluate the feasibility of using SFM as a road pavement material, a comprehensive discussion on the disinfecting and sterilizing methods is beyond the scope of this paper.

In this study, the thermal disinfection method was used to evaluate the disinfection influence on the property of masks and the unconfined compression strength of the blend. After heated in an oven at 75 °C, the measured elongation and tensile strength at break of the used masks were 118.91% and 3.63 MPa, respectively, slightly lower than those obtained from the clean/new masks (i.e., 118.96% and 3.97 MPa). The UCS value of the RCA sample containing 1% of the heated/shredded mask was observed at 210.8 kPa, approximately 2% lower than 216 kPa (UCS value of the new mask). Therefore, it can be stated that the thermal disinfection of the used masks has a minor effect on the strength and stiffness results.

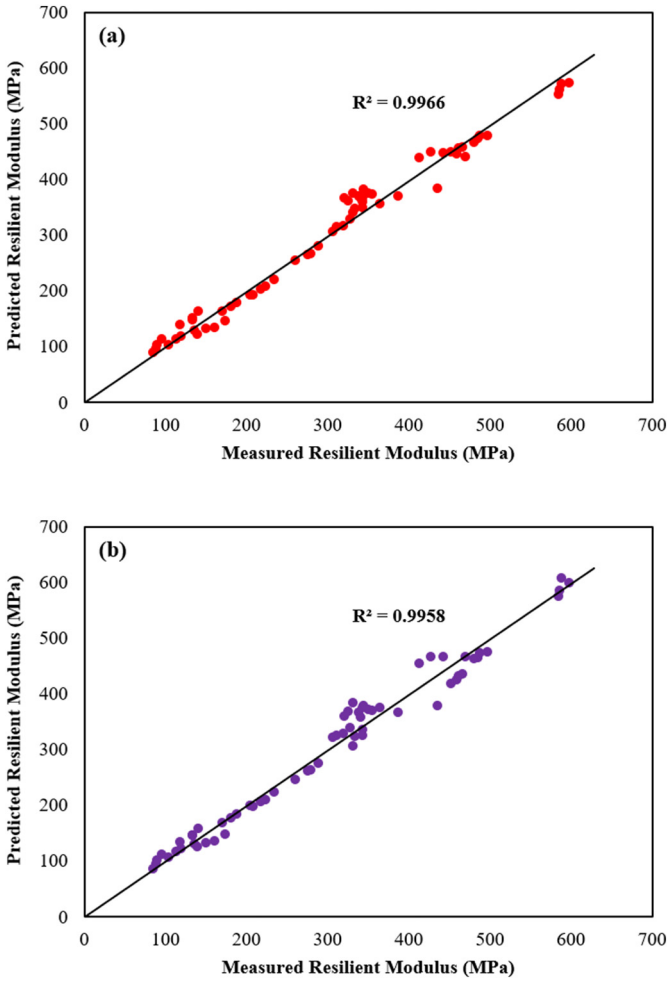

Fig. 5. Comparison of the measured M_r of the samples from the laboratory with the predicted M_r using (a) bulk-stress model and (b) three-parameter model.

5. Conclusions and future work

This paper proposed a new approach for reducing pandemic-generated waste by recycling the used surgical face masks with recycled concrete aggregate in pavements base/subbase layers. The following findings can be drawn from the experimental results of this study.

- The mixtures of SFM and RCA fitted within the upper- and lower-bound limits of the standard specifications for Type 1 gradation C materials for pavement base and subbase.
- The aggregate crushing value, Los Angeles abrasion and flakiness index of RCA were well below the maximum allowable limits for pavement base/subbase material recommended by the state road authorities.
- The SFM fibers were very light with a low specific gravity. The results of the tensile tests indicated the polypropylene layer of the masks contributed to most of the tensile strength. Moreover, the SFM fibers adopted in this study were classified as short or discontinuous fiber, which could provide better strength and stiffness.
- By increasing the SFM content, the OMC increased, while the MDD decreased. The reduction in the MDD was attributed to the lower specific gravity of SFM compared to that of the RCA.
- The inclusion of the SFM into RCA could provide more ductility and flexibility for the pavement base and subbase layers because of the higher tensile strength of SFM with more flexibility compared to the RCA particles.
- The addition of 1–2% SFM to RCA resulted in an increase in strength and stiffness of the blends of SFM/RCA. This is because SHM fibers played a reinforcing role in binding the RCA particles, and the bridging effect of the fibers in RCA could impede the further development of tension cracks. However, beyond 2%, increasing the amount of SFM resulted in a reduction in strength and stiffness. This was attributed to the fact that the excessive fiber inclusion led to the loss of strength and stiffness of the blended sample due to the high amount of voids.

- The optimal SFM content, which provided the highest UCS and M_r values, was found to be 1% of the dry weight of RCA.
- Overall, the blends of the waste materials (i.e., RCA and SFM), as a low carbon concept, satisfied the stiffness and strength requirements for pavements base/subbase; therefore, can be used as a viable and alternative base/subbase material.
- If 1% of SFM is added to RCA to make 1 km of a two-lane road with a width of 7 m and a thickness of 0.5 m for base and subbase, approximately 93.2 t of SFM would be required, i.e., preventing 3 million used face masks from ending up in landfills.
- Using SFM with RCA as an alternative pavement base/subbase material will not only reduce pandemic-generated waste and the need for virgin materials, but also reduce the construction costs significantly.

Given that most PPE is mainly made of plastics, including polypropylene, polyvinyl chloride and nitrile butadiene rubber, the proposed methodology can be applied to different PPE. A feasibility study, similar to one reported in this paper, needs to be conducted to investigate the potential use of other waste PPE with recycled concrete aggregate as pavement base/subbase materials. For future works, it is also recommended to assess the feasibility of using non-plastic face masks as another sustainable option to mitigate pandemic-generated waste.

CRediT authorship contribution statement

Mohammad Saberian: Methodology, Validation, Investigation, Writing – original draft, Data curation, Formal analysis, Visualization. **Jie Li:** Conceptualization, Writing – review & editing, Resources, Validation, Supervision, Project administration, Visualization. **Shannon Kilmartin-Lynch:** Writing – review & editing, Formal analysis, Visualization. **Mahdi Boroujeni:** Writing – review & editing, Formal analysis, Visualization.

Declaration of competing interest

We hereby confirm that there are no conflicts of interest associated with our paper.

Acknowledgements

The authors would like to acknowledge the financial support of the Lowitja Institute, Australia's national institute for Aboriginal and Torres Strait Islander health research.

Appendix A. Supplementary data

Supplementary data to this article can be found online at https://doi.org/10.1016/j.scitotenv.2021.145527.

References

AASHTO, 1993. AASHTO Guide for Design of Pavement Structures. American Association of State Highway Transportation Officials.
AASHTO, 2007. Standard method of test for determining the resilient modulus of soils and aggregate materials. AASHTO T307-99, Washington, DC.
AS 1141.15, 2018. Methods for Sampling and Testing Aggregates, Method 15: Flakiness Index. Australian Standard 1141.15. Australian Standard, Sydney, Australia, pp. 1–9.
AS 1141.21, 1997. Methods for Sampling and Testing Aggregates, Method 21: Aggregate Crushing Value. Australian Standard 1141.21. Australian Standard, Sydney, Australia, pp. 1–13.
AS 1141.23, 2009. Methods for Sampling and Testing Aggregates, Method 23: Los Angeles Value. Australian Standard 1141.23. Australian Standard, Sydney, Australia, pp. 1–13.
AS 1141.5.1, 2000. Particle Density and Water Absorption of Fine Aggregate. Australian Standard 1141.5.1, Sydney, Australia.
AS 1141.6.1, 2000. Methods for Sampling and Testing Aggregates, Method 6.1: Particle Density and Water Absorption of Coarse Aggregate-weighing-in-water Method. Australian Standard 1141.6.1. Australian Standard, Sydney, Australia, pp. 1–6.
AS 1289.3.6.1, 2009. Methods of Testing Soils for Engineering Purposes Soil Classification Tests - Determination of the Particle Size Distribution of a Soil - Standard Method of Analysis by Sieving. Australian Standard AS 1289.3.6.1. Australian Standard, Sydney, Australia.
AS 1289.4.3.1, 1997. Soil Chemical Tests-determination of the pH Value of a Soil-electrometric Method. Australian Standard 1289.4.3.1. Australian Standard, Sydney, Australia, pp. 1–5.
AS 1289.5.2.1, 2017. Soil Compaction and Density Tests-Determination of the Dry Density/Moisture Content Relation of a Soil Using Modified Compactive Effort. Australian Standard 1289.5.2.1. Australian Standard, Sydney, Australia, pp. 1–13.
AS 5101.4, 2008. Unconfined Compressive Strength of Compacted Materials. Australian Standard 5101.4. Australian Standard, Sydney, Australia, pp. 1–13.
ASTM D75-03, 2014. Standard Practice for Sampling Aggregates. ASTM International, West Conshohocken, PA.
ASTM D1241-15, 2015. Standard Specification for Materials for Soil-aggregate Subbase, Base, and Surface Courses. ASTM International, West Conshohocken, PA.
ASTM D2487-17, 2017. Standard Practice for Classification of Soils for Engineering Purposes (Unified Soil Classification System). ASTM D2487-17. ASTM International, West Conshohocken, PA.
ASTM D2974-14, 2014. Standard Test Methods for Moisture, Ash, and Organic Matter of Peat and Other Organic Soils. ASTM International, West Conshohocken, PA.
ASTM D570-98, 2018. Standard Test Method for Water Absorption of Plastics. ASTM International, West Conshohocken, PA.
ASTM D638-14, 2014. Standard Test Method for Tensile Properties of Plastics. ASTM International, West Conshohocken, PA.
ASTM D7138-16, 2016. Standard Test Method to Determine Melting Temperature of Synthetic Fibers. ASTM International, West Conshohocken, PA.
ASTM D792-20, 2020. Standard Test Methods for Density and Specific Gravity (Relative Density) of Plastics by Displacement. ASTM International, West Conshohocken, PA.
ASTM D854-10, 2010. Standard Test Methods for Specific Gravity of Soil Solids by Water Pycnometer. ASTM International, West Conshohocken, PA.
AzariJafari, H., Yahia, A., Amor, M.B., 2016. Life cycle assessment of pavements: reviewing research challenges and opportunities. J. Clean. Prod. 20 (112), 2187–2197.
Barcelo, D., 2020. An environmental and health perspective for COVID-19 outbreak: meteorology and air quality influence, sewage epidemiology indicator, hospitals disinfection, drug therapies and recommendations. Journal of Environmental Chemical Engineering 8 (4), 104006.
Bojnourdi, S., SheikhiNarani, S., Abbaspour, M., Ebadi, T., Mir Mohammad Hosseini, S.M., 2020. Hydro-mechanical properties of unreinforced and fiber-reinforced used motor oil (UMO)-contaminated sand-bentonite mixtures. Eng. Geol. 279, 105886.
Boroujeni, M., Saberian, M., Li, J., 2021. Environmental impacts of COVID-19 on Victoria, Australia, witnessed two waves of coronavirus. Environ. Sci. Pollut. Res. https://doi.org/10.1007/s11356-021-12556-y.
Chen, M., Shen, S.L., Arulrajah, A., Wu, H.N., Hou, D.W., Xu, Y.S., 2015. Laboratory evaluation on the effectiveness of polypropylene fibers on the strength of fiber-reinforced and cement-stabilized Shanghai soft clay. Geotext. Geomembr. 43 (6), 515–523.
Correia, A.A.S., Venda Oliveira, P.J., Custódio, D.G., 2015. Effect of polypropylene fibres on the compressive and tensile strength of a soft soil, artificially stabilised with binders. Geotext. Geomembr. 43 (2), 97–106.
Daryabeigi Zand, A., Vaezi Heir, A., 2020. Emerging challenges in urban waste management in Tehran, Iran during the COVID-19 pandemic. Resour. Conserv. Recycl. 162, 105051.
Dhawan, R., Bisht, B.M.S., Kumar, R., Kumari, S., Dhawan, S.K., 2019. Recycling of plastic waste into tiles with reduced flammability and improved tensile strength. Process Saf. Environ. Prot. 124, 299–307.
Doan, H.N., 2020. Medical face masks can be reused with microwave method: expert. https://vietnamnews.vn/society/654072/medical-face-masks-can-be-reused-with-microwave-method-expert.html.
Fadare, O.O., Okoffo, E.D., 2020. Covid-19 face masks: a potential source of microplastic fibers in the environment. Sci. Total Environ. 737, 140279.
Hajforoush, M., Madandoust, R., Kazemi, M., 2019. Effects of simultaneous utilization of natural zeolite and magnetic water on engineering properties of self-compacting concrete. Asian Journal of Civil Engineering 20 (2), 289–300.
Hamzavi, I.H., Lyons, A.B., Kohli, I., Narla, S., Parks-Miller, A., Gelfand, J.M., Lim, H.W., Ozog, D., 2020. Ultraviolet germicidal irradiation: possible method for respirator disinfection to facilitate reuse during COVID-19 pandemic. Journal of American Academy of Dermatalogy 82 (6), 1511–1512.
Hirsh, S., 2020. Every month, 200 billion face masks and gloves are going into the environment. Green matters. https://www.greenmatters.com/p/face-masks-gloves-litter-coronavirus.
Ibáñez-Cervantes, G., Bravata-Alcántara, J.C., Nájera-Cortés, A.S., Meneses-Cruz, S., et al., 2020. Disinfection of N95 masks artificially contaminated with SARS-CoV-2 and ESKAPE bacteria using hydrogen peroxide plasma: impact on the reutilization of disposable devices. Am. J. Infect. Control 48 (9), 1037–1041.
Ilyas, S., Srivastava, R.R., Kim, H., 2020. Disinfection technology and strategies for COVID-19 hospital and bio-medical waste management. Sci. Total Environ. 749, 141652.
IS 2386-4, 1963. Methods of Test for Aggregates for Concrete, Part 4: Mechanical Properties. Bureau of Indian Standards.
Jahandari, S., Saberian, M., Tao, Z., Mojtahedi, S.F., Li, J., Ghasemi, M., Rezvani, S.S., Li, W., 2019. Effects of saturation degrees, freezing-thawing, and curing on geotechnical properties of lime and lime-cement concretes. Cold Reg. Sci. Technol. 160, 242–251.
Kazemi, M., Hajforoush, M., Talebi, P.K., Daneshfar, M., Shokrgozar, A., Jahandari, S., Saberian, M., Li, J., 2020. In-situ strength estimation of polypropylene fibre reinforced recycled aggregate concrete using Schmidt rebound hammer and point load test. Journal of Sustainable Cement-Based Materials 1–18.
Klemeš, J.J., Fan, Y.V., Tan, R.R., Jiang, P., 2020. Minimising the present and future plastic waste, energy and environmental footprints related to COVID-19. Renew. Sust. Energ. Rev. 127, 109883.

Lei, B., Li, W., Tang, Z., Tam, V.W.Y., Sun, Z., 2018. Durability of recycled aggregate concrete under coupling mechanical loading and freeze-thaw cycle in salt-solution. Constr. Build. Mater. 163, 840–849.
Li, W., Luo, Z., Wu, C., Duan, W.H., 2018a. Impact performances of steel tube-confined recycled aggregate concrete (STCRAC) after exposure to elevated temperatures. Cem. Concr. Compos. 86, 87–97.
Li, J., Saberian, M., Nguyen, B.T., 2018b. Effect of crumb rubber on the mechanical properties of crushed recycled pavement materials. J. Environ. Manag. 218, 291–299.
Ludwig-Begall, L.F., Wielick, C., Dams, L., Nauwynck, H., Demeuldre, P.F., Napp, A., Laperre, J., Haubruge, E., Thiry, E., 2020. The use of germicidal ultraviolet light, vaporized hydrogen peroxide and dry heat to decontaminate face masks and filtering respirators contaminated with a SARS-CoV-2 surrogate virus. Journal of Hospital Infection 1–8.
Mishra, B., Gupta, M.K., 2018. Use of randomly oriented polyethylene terephthalate (PET) fiber in combination with fly ash in subgrade of flexible pavement. Constr. Build. Mater. 190, 95–107.
MolaAbasi, H., Saberian, M., Li, J., 2019. Prediction of compressive and tensile strengths of zeolite-cemented sand using porosity and composition. Constr. Build. Mater. 202, 784–795.
Naaman, A.E., 2003. Engineered steel fibers with optimal properties for reinforcement of cement composites. J. Adv. Concr. Technol. 1, 241–252.
Nzediegwu, C., Chang, S.X., 2020. Improper solid waste management increases potential for COVID-19 spread in developing countries. Resources, Conservation & Recycling 161, 104947.
Perera, S., Arulrajah, A., Wong, Y.C., Horpibulsuk, S., Maghool, F., 2019. Utilizing recycled PET blends with demolition wastes as construction materials. Constr. Build. Mater. 221, 200–209.
Pradhan, P.K., Kar, R.K., Naik, A., 2012. Effect of random inclusion of polypropylene fibers on strength characteristics of cohesive soil. Geotech. Geol. Eng. 30, 15–25.
Prata, J.C., Patrício Silva, A.L., Walker, T.R., Duarte, A.C., Rocha Santos, T., 2020. COVID-19 pandemic repercussions on the use and management of plastics. Environmental Science & Technology 54 (13), 7760–7765.
Puppala, A.J., Hoyos, L.R., Potturi, A.K., 2011. Resilient moduli response of moderately cement-treated reclaimed asphalt pavement aggregates. J. Mater. Civ. Eng. 23 (7), 990–998.
Rowan, N.J., Laffey, J.G., 2020. Unlocking the surge in demand for personal and protective equipment (PPE) and improvised face coverings arising from coronavirus disease (COVID-19) pandemic – implications for efficacy, re-use and sustainable waste management. Sci. Total Environ. 752, 142259.
Saberian, M., Li, J., 2018. Investigation of the mechanical properties and carbonation of construction and demolition materials together with rubber. J. Clean. Prod. 202, 553–560.
Saberian, M., Li, J., 2019. Long-term permanent deformation behaviour of recycled concrete aggregate with addition of crumb rubber in base and sub-base applications. Soil Dyn. Earthq. Eng. 121, 436–441.
Saberian, M., Li, J., 2021. Effect of freeze-thaw cycles on the resilient moduli and unconfined compressive strength of rubberized recycled concrete aggregate as pavement base/subbase. Transportation Geotechnics 27, 100477.
Saberian, M., Li, J., Cameron, D.A., 2019a. Effect of crushed glass on behavior of crushed recycled pavement materials together with crumb rubber for making a clean green base and subbase. J. Mater. Civ. Eng. 31 (7), 1–7.
Saberian, M., Li, J., Nguyen, B.T., Setunge, S., 2019b. Estimating the resilient modulus of crushed recycled pavement materials containing crumb rubber using Clegg impact value. Resour. Conserv. Recycl. 141, 301–307.
Saberian, M., Shi, L., Sidiq, A., Li, J., Setunge, S., Li, C.Q., 2019c. Recycled concrete aggregate mixed with crumb rubber under elevated temperature. Constr. Build. Mater. 222, 119–129.
Saberian, M., Li, J., Setunge, S., 2019d. Evaluation of permanent deformation of a new pavement base and subbase containing unbound granular materials, crumb rubber and crushed glass. J. Clean. Prod. 230, 38–45.
Saberian, M., Li, J., Boroujeni, M., Law, D., Li, C.Q., 2020a. Application of demolition wastes mixed with crushed glass and crumb rubber in pavement base/subbase. Resour. Conserv. Recycl. 156, 104722.
Saberian, M., Li, J., Nguyen, B.T., Boroujeni, M., 2020b. Experimental and analytical study of dynamic properties of UGM materials containing waste rubber. Soil Dyn. Earthq. Eng. 130, 105978.
Saberian, M., Li, J., Perera, S.T.A.M., Ren, G., Roychand, R., Tokhi, H., 2020c. An experimental study on the shear behaviour of recycled concrete aggregate incorporating recycled tyre waste. Constr. Build. Mater. 264, 120266.
Saberian, M., Li, J., Donnoli, A., Bonderenko, E., Oliva, P., Gill, B., Lockery, S., Siddique, R., 2021. Recycling of spent coffee grounds in construction materials: a review. J. Clean. Prod. 289, 125837.
Sangkham, S., 2020. Face mask and medical waste disposal during the novel COVID-19 pandemic in asia. Case Studies in Chemical and Environmental Engineering 2, 100052.
Silva, A.L.P., Prata, J.C., Walker, T.R., Campos, D., Duarte, A.C., Soares, A.M.V.M., Barcelò, D., Rocha-Santos, T., 2020. Rethinking and optimising plastic waste management under COVID-19 pandemic: policy solutions based on redesign and reduction of single-use plastics and personal protective equipment. Sci. Total Environ. 742, 140565.
Tang, C.S., Paleologos, E.K., Vitone, C., Du, Y.J., 2020. Environmental geotechnics: challenges and opportunities in the post-COVID-19 world. Environmental Geotechnics, 1–21 https://doi.org/10.1680/jenge.20.00054.
Tomar, A., Sharma, T., Singh, S., 2020. Strength properties and durability of clay soil treated with mixture of nano silica and polypropylene fiber. Materials Today Proceedings 26 (3), 3449–3457.
Venda Oliveira, P.J.V., Correia, A.A.S., Cajada, J.C.A., 2018. Effect of the type of soil on the cyclic behaviour of chemically stabilised soils unreinforced and reinforced with polypropylene fibres. Soil Dyn. Earthq. Eng. 115, 336–343.
VicRoads, 2017. Registration for Crushed Rock Mixes, Code of Practice RC 500.02. VicRoads, Melbourne.
Xiang, Y., Song, Q., Gu, W., 2020. Decontamination of surgical face masks and N95 respirators by dry heat pasteurization for one hour at 70°C. Am. J. Infect. Control 48 (8), 880–882.
Yaghoubi, E., Arulrajah, A., Wong, Y.C., Horpibulsuk, S., 2017. Stiffness properties of recycled concrete aggregate with polyethylene plastic granules in unbound pavement applications. Journal of Materials in Civil Engineering 29 (4), 04016271 (1-7).
Zaimoglu, A.S., 2010. Freezing-thawing behavior of fine-grained soils reinforced with polypropylene fibers. Cold Reg. Sci. Technol. 60 (1), 63–65.
Zambrano-Monserrate, M.A., Ruano, M.A., Sanchez-Alcalde, L., 2020. Indirect effects of COVID-19 on the environment. Sci. Total Environ. 728, 138813.